PHYSICAL REVIEW B VOLUME 2, NUMBER 3 1 AUGUST 1970

# Ultrasonic Attenuation in a Superconducting Vanadium-Tantalum Alloy

B. R. Tittmann

*Science Center, North American Rockwell Corporation, Thousand Oaks, California* 91360
(Received 16 October 1969)

Ultrasonic-attenuation measurements have been carried out on the magnetically reversible, type-II superconductor V – 5.6-at.% Ta with both a high Ginzburg-Landau parameter ($\kappa_G \approx 5$) and the Bardeen, Cooper, and Schrieffer (BCS) coherence length 5 times the electronic mean free path. The electronic attenuation $\alpha$ in zero magnetic field below $T_c$ is BCS-like, giving a zero-temperature energy gap $2\Delta_0(0, 0) \approx 3.6 k_B T_c$, and in the normal state has the theoretically predicted dependence on $q$ and $l$. The upper critical field $H_{c2}$ could be deduced from the attenuation data to an accuracy better than 1%, and its temperature dependence agrees well with type-II theory without $p$-wave scattering of electrons. Use of the measured normal-state resistivity and ultrasonically determined values of $T_c$, $H_{c2}(T)$, and $\partial\alpha/\partial H$ at $H = H_{c2}$ inserted in an ultrasonic-attenuation theory due to Maki enabled the calculation of an Abrikosov-Maki parameter $\kappa_2$, which agreed roughly with the $\kappa_2$ obtained in previous magnetic and calorimetric measurements. Thus, for $H$ close to $H_{c2}$, the data agree with Maki's dirty-limit ($\xi_0/l \gg 1$) theory, which predicts a linear dependence of $\alpha$ on $H$. At fields farther from $H_{c2}$, $\alpha(H)$ deviates from linearity and appears to fit empirically a parabolic function of $H$. At very low fields $H \gtrsim H_{c1}$, the $H$ and $T$ dependence of $\alpha$ is in apparent agreement with another theory. Physical insight into the behavior in this region could be obtained with a model in which vortices are replaced by cylinders of completely normal material imbedded in a superconducting matrix.

## I. INTRODUCTION

Much theoretical[1-7] and experimental[8-19] work has been carried out on ultrasonic attenuation in clean type-II superconductors characterized by having an electronic mean free path greater than the BCS coherence length, $l > \xi_0$, and having a small Ginzburg-Landau parameter $\kappa_G \approx 1$. Although there have been theoretical studies[7,20-23] of the dirty regime characterized by $l < \xi_0$ and $\kappa_G > 1$, only few experimental investigations[13,24] have been reported and discussed in the light of recent theory. One[24] of these is confined to alloys with extremely high upper critical fields $H_{c2}$ and does not study the electron-phonon interaction which is basic to this investigation. The other experiment,[13] performed on the alloy Mo – 25-at.% Re ($\kappa_G \cong 4$), yielded a linear dependence of the electronic attenuation $\alpha$ on magnetic field near $H_{c2}$ in qualitative agreement with the dirty-limit theory,[7,21,22] although the measured slope $\partial\alpha/\partial H$ was in disagreement with its predicted value. For the region in which $H \ll H_{c2}$, no mention was made of the degree of magnetic reversibility and no interpretation was given for the ultrasonic data.

The present experiments were undertaken to see whether a more quantitative comparison with the theory[7,21,22] was feasible, and in particular, to explore the region in which $H \ll H_{c2}$, where few data for the electronic attenuation in the dirty regime are available. For this purpose, a single crystal of a well-characterized magnetically reversible type-II superconductor with reasonable $T_c$ and $H_{c2}$ values and moderately high $\kappa_G$ and $\xi_0/l$ values was necessary. These requirements could be fulfilled with the solid-solution alloy V – 5.6-at.% Ta and single oriented crystals of this composition were grown by Nadler of this laboratory. Previous calorimetric[25] and magnetization[26] studies and the present resistivity and ultrasonic data combine to render the alloy a well-characterized metal with $T_c = 4.7\,^\circ\mathrm{K}$, $H_{c2}(T=0) \approx 10$ kG, $\kappa_G \approx 5$, and $\xi_0/l \approx 5$. The ultrasonic measurements[27] display a substantial electron-phonon interaction, magnetic reversibility, well-defined (to better than 1%) upper critical fields $H_{c2}$, and a behavior consistent with previous studies[25,26] so that a quantitative comparison with theory is possible. The absence of hysteresis (except near $H = 0$) means that the field-dependent attenuation in the range $H \ll H_{c2}$ is physically significant, so that its magnitude and temperature dependence should be amenable to detailed analysis and quantitative interpretation.

The field dependence of the attenuation can, in principle, define the lower and upper critical fields, $H_{c1}$ and $H_{c2}$. It is of interest to compare the observed temperature dependence of $H_{c2}$ with that predicted by recent type-II theories.[28-30] Very little experimental information is available on $H_{c1}$, partly because demagnetization effects and

flux trapping often cause the field of first flux penetration to deviate from the ideal $H_{c1}$. Efforts were made to achieve a small demagnetization factor suitable for $H_{c1}$ measurements by placement of the cylindrical sample in between long sections of polycrystalline material of nominally V – 5.6-at. % Ta composition. Also, care was taken in the growth and preparation of the crystals to remove as many flux trapping centers as possible.

## II. APPARATUS AND SAMPLE PREPARATION

The apparatus and measurement techniques used in this experiment are essentially the same as those already described elsewhere,[31] except for some modifications described below. Sample shape is well known to influence the initial flux penetration field $H_{fp}$ and the slope[32,33] of the magnetization curve near $H_{c2}$. The latter is especially affected when the condition[33] $(2\kappa_2^2 - 1)\beta \gg 1$ is not satisfied, where $\beta$ is a numerical constant of order unity and $\kappa_2$ is the Abrikosov-Maki parameter the value of which may be the objective of a magnetization measurement. Similarly, the magnetic field dependence of the ultrasonic attenuation should be somewhat shape dependent. In the case of V – 5.6-at. % Ta, the parameter $\kappa_2$ ranges from five to six so that the above condition is indeed satisfied. To achieve a small uniform demagnetization field, the sample cavity was modified, as described in the Appendix, and the cylindrical sample (length $L = 3.8$ cm, diameter $D = 1.3$ cm) was placed in between tapered cylindrical conductors machined from polycrystalline material of nominally V – 5.6-at. % Ta composition. Therefore, except for the presence of the transducers (0.025 cm thick), the configuration presented approximately the same material over a total length of about 15 cm and had an estimated effective demagnetization factor[34] $n_{\text{eff}} \approx 0.015$. Furthermore, transducers of diameter smaller than that of the sample were used in order to confine the beam of propagating sound waves to the interior of the sample. Thus, perturbations from the side surface and any effects from distortions of the flux lines, particularly near the sample ends, were hopefully minimized.

Most of the measurements were performed on samples obtained from the single crystal described below. The measurements performed on samples from other crystals show qualitatively the same features, although the values of such quantities as the upper critical field $H_{c2}$, the transition temperature $T_c$, the normal-state resistivity $\rho_n$, and the Abrikosov-Maki parameter $\kappa_2$ differed slightly from crystal to crystal. Variations in composition and purity of source material are thought to account for these differences.

The crystals were grown by Nadler of this laboratory. To prepare the V – 5.6-at. % Ta single crystal, the source material (electron-beam zone refined capacitor grade 99.9%-pure tantalum and electro-refined 99.98%-pure vanadium supplied by the U.S. Bureau of Mines) was consolidated into a homogeneous $\frac{5}{8}$-in.-diam ingot by conventional nonconsumable-electrode arc-melting techniques and then swaged to a $\frac{1}{2}$-in.-diam rod. The electron-beam floating-zone method was used to grow a seed crystal from which a [110]-oriented specimen was grown. Three zone traverses were made at a traverse rate of 6.8 in./hr; subsequent analysis by wet chemistry techniques showed a composition of V – (5.6±0.2)-at. % Ta at both ends of the crystal. The internal stress resulting from the growth process was minimized by the annealing of the crystal for 30 min at 1500 °C in a $4 \times 10^{-6}$ Torr vacuum. Metallographic analysis, by optical and electron microscopy, showed only dislocation tangles and etch pits. Chemical analysis results showed about 500 ppm (parts per million by weight) of dissolved gases (H, O, N), 33 ppm of C, 100 ppm of Cr, and no other detectable elements.

The Laue back-reflection x-ray method served to orient the specimens crystallographically for slicing by a diamond saw. Subsequent mechanical polishing and a final mechanical-chemical polish[35] produced end surfaces (a) flat to better than 1000 Å, (b) parallel to 7 seconds, (c) crystallographically oriented within 1°, and (d) damage free as determined by Laue back-reflection x-ray patterns.

## III. RESULTS

### A. Normal State

A large attenuation due to electron-phonon interaction is well known to occur in normal-state single-crystal metals when the temperature is lowered into the liquid-helium range.[36] The interaction depends on the relative values of the sound wave number $q$ and the electron mean free path $l$. The latter may be estimated from the expression[37,38]

$$l = 1.27 \times 10^4 [\rho_n n^{2/3} (S/S_F)]^{-1} \quad , \tag{1}$$

where $\rho_n(\Omega\,\text{cm}) \equiv$ normal-state resistivity $= 4.1 \times 10^{-6}\ \Omega\,\text{cm}$, $n$ is the conduction-electron density, and $S/S_F$ is the ratio of the free area of the Fermi surface to the area of the Fermi surface for a free-electron gas of density $n$. The usual[39] assumption that $n$ is the average number of "valence" electrons (number of electrons outside closed shells) gives $n \approx 3.6 \times 10^{23}$ electrons/cm$^3$. Making the usual[25,39,40] rather uncertain assumption $(S/S_F) \approx 0.6$ for transition metals yields the value $l \approx 1.0 \times 10^{-6}$ cm. From the measured velocity of sound, $v_s = 6.2 \times 10^5$ cm/sec, and the center operating frequency $\omega \approx 6.3 \times 10^9$ rad/sec, the value $q = \omega/v_s \approx 1.0 \times 10^4$ per cm is estimated, and, therefore, $ql \approx 0.01$.

Using a free-electron classical method (except for the use of the Fermi distribution), Pippard[41] calculated the electronic attenuation $\alpha$ which for the present case of longitudinal waves in the regime $ql<1$ reduces to

$$\alpha \propto (mnv_F/v_s\mu)\, q^2 l \ , \qquad (2)$$

where $m$ is the electron mass, $v_F$ is the Fermi velocity, and $\mu$ is the mass density. Equation (2) gives the same dependence on $q$, $l$, and $v_s$ as a recent more general derivation, taking into account real metal effects.[42] The frequency dependence of the electronic attenuation observed for V – 5.6-at.% Ta (where the frequency $\nu = qv_s/2\pi$) was found to be in reasonable agreement with that predicted by Eq. (2) over the 0.5 – 2.0-GHz frequency range examined for this dependence. This agreement establishes some confidence in the value for the parameter $l$ obtained from Eq. (1).

The electronic attenuation extrapolated to zero temperature was found to be $\alpha \approx 2.9$ dB/cm at $\nu \approx 1.0$ GHz. This value was obtained, as indicated in Fig. 1, by subtracting the attenuation in the zero-$H$ superconducting state near $T = 0$ °K from that in the normal state at the same temperature. Such a procedure is believed valid because, as described in Sec. III B, at $T = 0$ °K the electronic contribution to the attenuation is predicted[43,44] to be zero in the superconducting state.

Equation (2) predicts a linear dependence of the electronic attenuation on the mean free path $l$ of the conduction electrons. As is well known, in many pure metal crystals, $l$ is found to increase as the temperature is lowered into the liquid-helium range ($l \sim T^{-5}$). In agreement with Eq. (2), the attenuation is likewise observed to increase with decreasing temperature in these crystals. In contrast, in V – 5.6-at.% Ta the attenuation was observed to be constant with temperature as seen in Fig. 1. This must be expected, however, since the mean free path is limited by the temperature-independent atomic disorder characteristic of a random solid-solution alloy.

### B. Superconducting State

When the temperature is lowered below $T_c$ in zero field, the attenuation due to the electron-phonon interaction drops abruptly and goes to zero as the temperature is lowered further. BCS[43] predict for the ratio of the electronic attenuation in the superconducting state $\alpha_s$ to the zero-field electronic attenuation $\alpha_n$ that would be present in the normal state if the specimen did not become superconducting

$$\alpha_{sm}/\alpha_n = 2\{\exp[\Delta_0(0, T)/k_B T] + 1\}^{-1} \ , \qquad (3)$$

where from Fig. 1 $\alpha_n(\mathrm{BCS}) = \alpha(T > T_c) = \alpha(H = H_{c2}, T) \equiv \alpha_n$, $\Delta_0(0, T)$ is the superconducting half-energy gap, and $k_B$ is Boltzmann's constant. Equation (3) was orginally derived for $ql > 1$ and $\Delta_0(0, T) \gg \hbar\omega$ (the phonon energy), but subsequently has been shown[44] to hold for all values of $ql$ for longitudinal waves. Since $\Delta_0(0, T) \approx 10^{12}$ Hz, in comparison to the center operating frequency of $10^9$ Hz, the above inequality is satisfied except in the region very near to $T = T_c$, a study of which was considered outside the scope of this investigation. With the help of Eq. (3) and the tables of $\Delta_0(0, T/T_c)/\Delta_0(0, 0)$ of Mühlschlegel,[45] the temperature dependence of $\alpha_{sm}/\alpha_n$ was calculated and compared with that observed. The usual[36] method was employed of varying the temperature-independent background attenuation $\alpha_B$ until that background was found which, when subtracted from the data, gave the best fit to the BCS temperature dependence of the attenuation ratio. As displayed in Fig. 1, fair agreement was found between the calculated (solid line) and the experimental temperature dependence for a choice of $2\Delta_0(0, 0) = 3.6\, k_B T_c$. An investigation was also made of how the curves in Fig. 1 change shape with frequency. Theory[44] predicts no change with frequency for longitudinal waves and no gross changes were observed here. The changes that have been observed by others[36,46] in the regime of $ql \ll 1$ have been small and were considered outside the scope of this investigation. The absence of pronounced changes of shape with

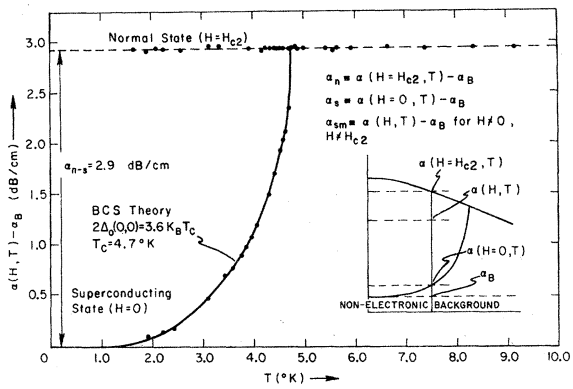


FIG. 1. Temperature dependence of the attenuation in the normal and superconducting state of V – 5.6-at.% Ta at 1.0 GHz for longitudinal waves along the ⟨110⟩ direction. The normal-state measurements below $T_c$ were obtained in the presence of a magnetic field $H > H_{c2}$. The following symbol convention is adopted: $\alpha(H, T)$ = measured attenuation at given field $H$ and temperature $T$, $\alpha_n$ = normal electronic, $\alpha_s$ = superconducting electronic, $\alpha_{sm}$ = mixed state electronic, and $\alpha_B$ = nonelectronic attenuation independent of $H$ and $T$. [$2\Delta_{00} \equiv$ superconducting energy gap in zero field and at absolute zero in temperature $\equiv 2\Delta_0(0, 0)$.]

frequency indicates that the attenuation in the superconducting state for $T \neq 0$ has nearly the same frequency dependence as in the normal state, i.e., frequency squared.

### C. Mixed State

Figure 2 shows a typical example of the attenuation versus magnetic field data. The attenuation was measured by the pulse method at frequencies from one-half to three GHz for *longitudinal waves parallel* to the *applied magnetic* field. The magnetic field of initial flux penetration, $H_{fp}$, is clearly defined and the attenuation increase in the vortex state, $H_{fp} < H < H_{c2}$, is presumably associated with the attenuation caused by an apparent spatially varying periodic energy gap. The upper critical field $H_{c2}$ is clearly defined by the attenuation data both for increasing and decreasing fields. The only hysteresis is near $H = 0$ where some flux trapping can be expected. Most of the features described above for Fig. 2 are temperature dependent as, for example, $H_{fp}$ and $H_{c2}$ which are shown in Fig. 3 as derived from similar attenuation curves obtained at different temperatures. Some irreversibility and irregularity, shown in Fig. 2 in the vicinity of $H_{fp}$, suggests, however, that $H_{fp}$ may be somewhat larger than the ideal lower critical field $H_{c1}$. The irregularity may in part be the result of the polycrystalline V – 5.6-at. % Ta tapered conductors (see Sec. II) having a slightly different value of $H_{fp}$ compared to that of the sample. Except near $H = H_{fp}$, the magnetic field values $H$ are approximately equal to the values of the flux density $B$, i.e., $B = 4\pi M + H \approx H$. This is a consequence of the high value of the Abrikosov-Maki parameter $\kappa_2$ for this material ($\kappa_2 \gtrsim 5$); e.g., in Fig. 2 at $H = 0.2 H_{c2} \approx 0.94$ kOe the definition of $\kappa_2$ gives $|4\pi M| = (H - H_{c2})/(2\kappa_2^2 - 1)\beta \approx 65$ Oe, so that the approximation $B \approx H$ has an error of about 7%. At higher $H$, this error becomes much smaller.

#### 1. *Temperature Dependence of* $H_{c2}$

Recent theory[28–30] treats the temperature dependence of $H_{c2}$ for the range of purity values ($0 \leq \xi_0/l \leq \infty$) and includes[30] both $s$-wave and $p$-wave scattering of the conduction electrons by impurities. The purity parameter $\xi_0/l$ for V – 5.6-at. % Ta was obtained from the estimate of $l$ by Eq. (1) and the estimate of the BCS coherence length $\xi_0$ from the

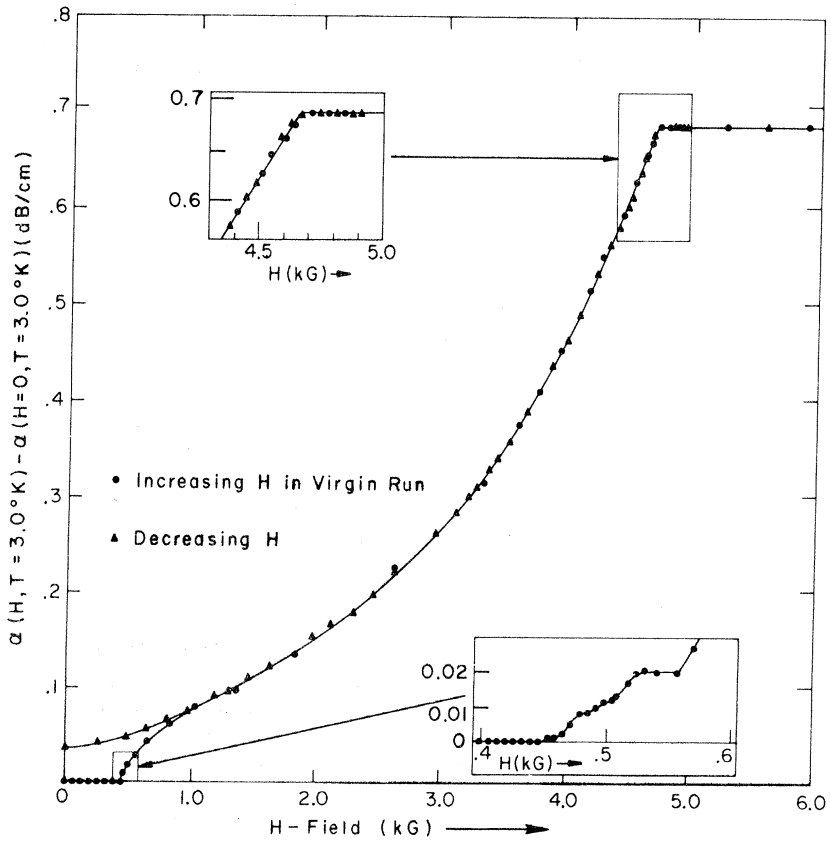


Fig. 2. Measured attenuation $\alpha(H, T = 3.0°\text{K}) - \alpha(H = 0, T = 3.0°\text{K})$ at 0.54 GHz as a function of applied magnetic field $H$ parallel to longitudinal sound waves in V – 5.6-at. % Ta ($\xi_0/l \approx 5$). The regions near the initial flux penetration field $H_{fp} = 0.45$ kG and the upper critical field $H_{c2} = 4.67$ kG are shown expanded.

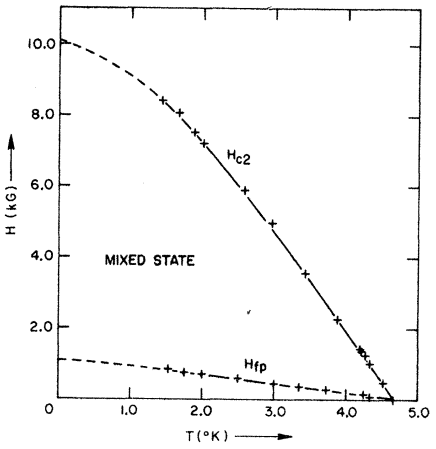


FIG. 3. Temperature dependence of initial flux penetration field $H_{fp}$ and upper critical field $H_{c2}$ as obtained from ultrasonic measurements for V – 5.6-at. % Ta.

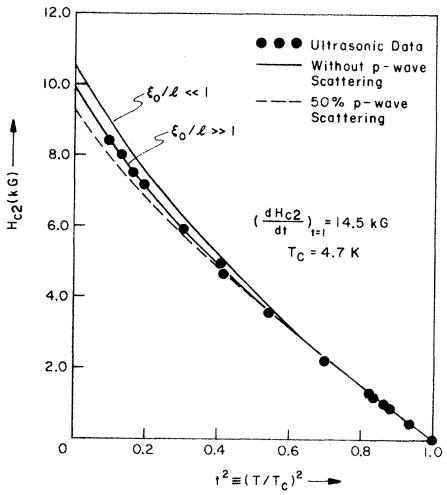


FIG. 4. Temperature dependence of $H_{c2}$ as obtained from ultrasonic measurements (solid circles) compared with type-II theories (solid and dashed lines).

expression[37–39]

$$\xi_0 \approx 7.93 \times 10^{-17} n^{2/3} (S/S_F)(\gamma T_c)^{-1} \ , \qquad (4)$$

where $\gamma$(erg cm$^{-3}$ °K$^{-2}$) is the electronic specific-heat coefficient. Use of the same values for $n$ and $(S/S_F)$ as in the estimate for $l$ and of the previously measured[25] value for $\gamma = 1.10 \times 10^4$ ergs cm$^{-3}$ °K$^{-2}$ corrected[47] for differences in $T_c$ of the specimens, gives $\xi_0 \approx 4.6 \times 10^{-6}$ cm and, therefore, a purity parameter $\xi_0/l \approx 5$. For this value the theory for $s$-wave scattering predicts[28,29] essentially dirty-limit behavior of $H_{c2}$. Figure 4 shows the theoretical curves for the dirty and clean limits and also the approximate curve[30] for equal contribution of $s$-wave and $p$-wave scattering for $\xi_0/l = 4$. [The theory[28,29] gives $h^* \equiv H_{c2}(t)/(-dH_{c2}/dt)_{t=1}$; the solid curve in Fig. 4 gives $H_{c2}(t) = h^*$ (theor) $\times (-dH_{c2}/dt)_{t=1}$(expt), where $t = T/T_c$.] The $H_{c2}$ data of Fig. 3 have been replotted on Fig. 4 and show good agreement with dirty-limit theory for *little or no p-wave scattering*.

### 2. *Temperature and Frequency Dependence of Attenuation*

Figure 5 compares data for the field dependence of the attenuation for various temperatures by plotting reduced values of the field-dependent electronic attenuation $[\alpha(H,T) - \alpha(H=0,T)]/[\alpha(H=H_{c2},T) - \alpha(H=0,T)] = [\alpha_{sm} - \alpha_s]/[\alpha_n - \alpha_s]$ as a function of the reduced field $h' = H/H_{c2}$. A marked feature of this comparison is that as the temperature is lowered from $T_c$ the curves change shape. Hysteresis is unlikely to play a role in this behavior, since the curves are reversible except near and below $H_{fp}$. A study of the field-dependent electronic attenuation curve near $T_c$, i.e., $t \equiv T/T_c \approx 0.9$, as a function of frequency revealed that the shape of the curve remained about the same as the frequency was changed by a factor of 4, as shown in Fig. 6. As indicated in Sec. III A, the frequency dependence of the electronic attenuation for the

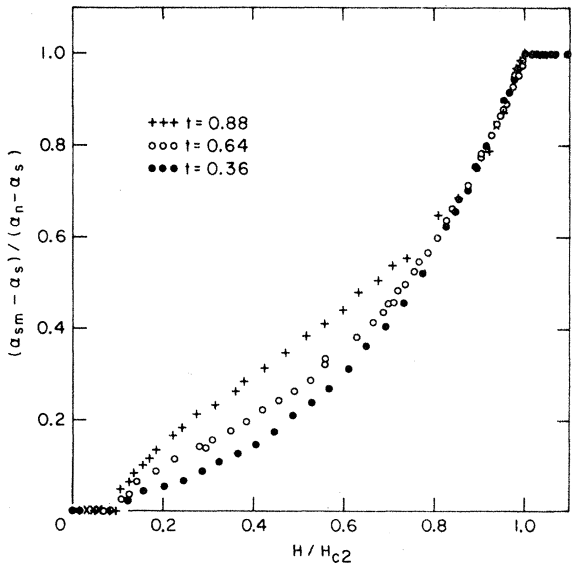


FIG. 5. Electronic attenuation $[\alpha(H,T) - \alpha(H=0,T)]/[\alpha(H=H_{c2},T) - \alpha(H=0,T)]$ or $(\alpha_{sm} - \alpha_s)/(\alpha_n - \alpha_s)$ as function of field for several temperatures at same frequency 0.54 GHz. Note change in curve shape as function of temperature.

present specimen in the normal state is proportional to the square of the frequency as expected from normal electron-phonon interaction. The fact that the attenuation curve in Fig. 6 shows no systematic change as a function of frequency, indicates that the mechanism responsible for the shape and over-all level of attenuation in the mixed state also has a square-law frequency dependence. This is, generally, similar to the frequency dependence of the electronic attenuation observed in the zero-field superconducting state as described in Sec. III B.

### 3. *Ultrasonic Attenuation for $H \lesssim H_{c2}$*

A theoretical expression for the electronic attenuation of longitudinal sound waves $\alpha' = \alpha_{sm}/\alpha_n = [\alpha(H, T) - \alpha_B]/[\alpha(H = H_{c2}, T) - \alpha_B]$ as a function of applied magnetic field $H$ near $H_{c2}$ is given[7,21,22] for the limit $\xi_0/l \gg 1$ by

$$\alpha' = 1 - \frac{e\rho_n c}{8\pi^2 k_B T_c} \frac{H_{c2} - H}{[2\kappa_2^2(t) - 1]\beta} C_2(t) \quad , \tag{5}$$

where $C_2(t)$ is a universal function[7] of the reduced temperature $t \equiv T/T_c$, $e$ is the electronic charge, $k_B$ is Boltzmann's constant, $c$ is the speed of light, and $\beta = 1.16$. In order to verify Eq. (5), the Abrikosov-Maki parameter $\kappa_2$ was calculated from the data and compared with values obtained in previous[25,26] studies. In terms of the slope at $H_{c2}$ of the field-dependent attenuation curve, the parameter $\kappa_2$ may be written as

$$\kappa_2^2 = \frac{1}{2} + \frac{ec\rho_n C_2(t)}{16\pi^2 k_B T_c \beta \partial\alpha'(t)/\partial H} \quad . \tag{6}$$

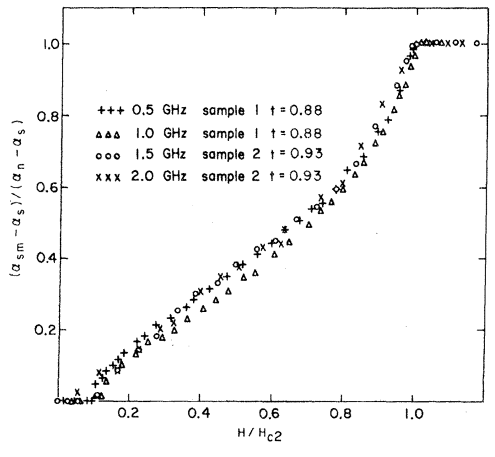


FIG. 6. Electronic attenuation $(\alpha_{sm} - \alpha_s)/(\alpha_n - \alpha_s)$ for several frequencies at the same temperature. Note absence of any systematic shape change of curve with frequency.

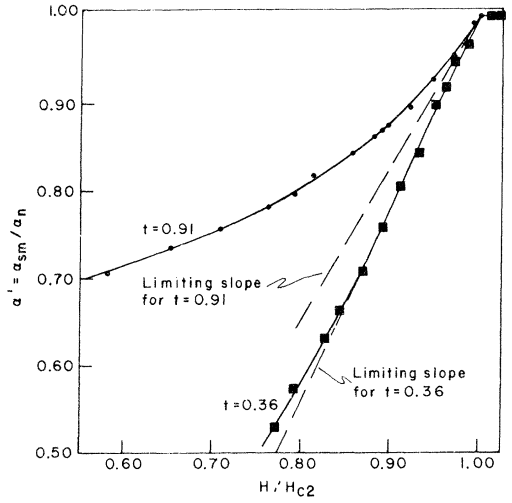


FIG. 7. Electronic attenuation $\alpha' = [\alpha(H, T) - \alpha_B]/[\alpha(H = H_{c2}, T) - \alpha_B] = \alpha_{sm}/\alpha_n$ near $H_{c2}$ for two temperatures. The slopes of the curves at $H_{c2}$ yield the value and temperature dependence of the Abrikosov-Maki parameter $\kappa_2$.

From the measured values of $\rho_n$, $T_c$, the numerical values[7] of $C_2(t)$, the observed slopes, and Eq. (6) the parameter $\kappa_2$ was calculated. Figure 7 shows typical data from which $\partial\alpha'(t)/\partial H$ was obtained for this calculation. Specifically, it shows the field-dependent electronic attenuation $\alpha' = \alpha_{sm}/$ magnetization[26] data on V-Ta alloys of similar composition. For $t \approx 1$ the accuracy of $\partial\alpha'(t)/\partial H$ at $H = H_{c2}$ is limited, because of the limited region for which the curve is linear. The extrapolation to $t = 1$ of the values of $\kappa_2(t)$, obtained from the slopes of the curves in Fig. 7 and Eq. (6), yields $\kappa_2(t = 1) = \kappa_G \approx 4.7$. A comparison with theory[7,21,22] of the temperature dependence of $\kappa_2$ shows agreement for $\xi_0/l \approx 5$ without $p$-wave scattering. The parameter $\kappa_G$ may also be estimated as follows[40]:

$$\kappa_G = \kappa_0 + \kappa_l \quad , \tag{7}$$

where the intrinsic contribution is

$$\kappa_0 = 1.61 \times 10^{24} \gamma^{3/2} T_c [n^{4/3}(S/S_f)^2]^{-1} \tag{8}$$

and the extrinsic contribution is

$$\kappa_l = 7500 \rho_n \gamma^{1/2} \quad . \tag{9}$$

The same estimates for $(S/S_f)$ and $n$, as were described above, and the measured values for $\rho_n$, $\gamma$, and $T_c$, gave for the intrinsic contribution $\kappa_0 \approx 1.0$, and for the extrinsic contribution $\kappa_l \approx 3.5$. Thus, $\kappa_G \approx 4.5$ in fair agreement with the $\kappa_G = 4.7$ value based on the ultrasonic data. The fact that the combination of the ultrasonic-attenuation theory and experiment is capable of yielding reasonable

$\kappa_2$ values with a qualitatively correct temperature dependence of $\kappa_2$ is remarkable, especially considering the relative complexity of the theory. This result and the results for $H_{c2}$ point to the ultrasonic technique as being a useful and sensitive tool for the investigation of type-II superconductors, especially in view of the well-known advantage of the technique, in that it can probe the bulk interior of the specimen.

### 4. *Ultrasonic Attenuation for* $H_{fp} < H < H_{c2}$

Theory predicts a parabolic[3] dependence of the attenuation on the applied field near $H_{c2}$ for $\xi_0/l \ll 1$, i.e., $1-\alpha' \propto (1-h')^{1/2}$, and a linear[7,21,22] dependence [see Eq. (5)] for $\xi_0/l \gg 1$, i.e., $1-\alpha' \propto (1-h')$, where $\alpha' \equiv \alpha_s/\alpha_n$ and $h' \equiv H/H_{c2}$. The present data can be considered in agreement with the latter prediction (see Fig. 9) for $H$ just below $H_{c2}$. However, for somewhat lower $H$, the field-dependent electronic attenuation deviates from linearity. Because the data are reversible and were obtained point by point with five-minute time spans to allow equilibration at a temperature maintained to one millidegree, this behavior is believed to be real and beyond experimental error. The theoretical solution for $\xi_0/l \gg 1$ indicates that near $H_{c2}$ the absorption $1-\alpha'$ should be proportional to the spatial average of square of the order parameter, $\langle|\Psi|^2\rangle$, which is also proportional to the magnetization. Both theoretical predictions[48] and experimental data on magnetization curves for dirty type-II superconductors show long linear regions[49] (down to $H/H_{c2} \approx 0.5$ for $\kappa_G \approx 5$) in contrast

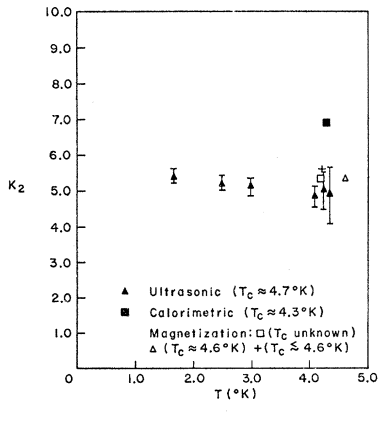


FIG. 8. Values for parameter $\kappa_2$ as a function of temperature. The present ultrasonic values of $\kappa_2$ in V – 5.6-at. % Ta are compared with those obtained in previous calorimetric (Ref. 25) and magnetization (Ref. 26) studies on polycrystalline samples of nominally V – 5-at. % Ta composition.

to the behavior observed for $\alpha'(H)$. While present theory treats on a quantitative basis only the pure[3] ($\xi_0/l \ll 1$) and dirty[7,21,22] ($\xi_0/l \gg 1$) limits, recent theoretical work[4,49] examines on a qualitative basis intermediate values of $\xi_0/l$. One treatment[4] considers the case of a nearly pure type-II superconductor in a sufficiently high magnetic field, such that $k_c l \gg 1$, where $k_c = (H/\phi_0)^{1/2}$ and $\phi_0 = hc/2e = 2.067 \times 10^{-7}$ G cm$^2$ is the fluxoid quantum. The pure-limit solution[3] is concluded to hold only for the range of fields considerably below $H_{c2}$, where $(k_c l)^2(H_{c2}-H)/H_{c2} \gg 1$. At the high-field end of this range the solution is thought to gradually change from that of the pure limit to that of the dirty limit. Very near $H_{c2}$ there is thought to be a region, where $(k_c l)^2(H_{c2}-H)/H_{c2} \ll 1$, and where the attenuation is indeed proportional to $(1-h')$. Although in the present experiment typically $k_c l \approx 0.01$, so that the above treatment is not applicable, the data are consistent with a description which defines two regions: a linear region near $H_{c2}$ where $1-\alpha' \propto (1-h')$ and a parabolic region for lower fields $H$ where $1-\alpha' \propto (1-h')^{1/2}$. Figure 7, which is a plot of $(1-\alpha')$ versus $(1-h')$, displays linear segments just below $H = H_{c2}$; while Fig. 10, which plots $(1-\alpha')$ versus $(1-h')^{1/2}$, shows that the data for $H \ll H_{c2}$ fall on straight lines over substantial ranges of field, indicating a $(1-h')^{1/2}$ dependence. Another treatment[49] for intermediate $\xi_0/l$ concludes the linear dependence to hold in the regime $(H_{c2}-H)/H_{c2} \ll [(\xi_0/l)(1-T/T_c)]^2$. Figure 7 reveals that the length of the linear segment below $H_{c2}$ increases as the temperature is lowered from $T_c$. The linear regions extend down to nearly $0.83H_{c2}$ from $H_{c2}$ at $T = 0.36T_c$, down to nearly $0.94H_{c2}$ at $T = 0.64T_c$ and are almost absent at $T = 0.91T_c$. This temperature dependence is in qualitative agreement with the above criterion[49] for the estimated $\xi_0/l \approx 5$.

A treatment, that has been used for interpreting ultrasonic[8,14,15] specific heat,[25] and thermal conductivity[50] data, is the "effective energy-gap approximation." This treatment is based on (a) the prediction of the Abrikosov[51] theory that the magnetization $M$ near $H_{c2}$ is proportional to the square of the order parameter, $M \propto \langle|\Psi|^2\rangle$, and (b) the assumption that the effective energy gap is proportional to the root mean square of the order parameter $\overline{\Delta}_0 \propto \langle|\Psi|^2\rangle^{1/2}$. For moderately high $\kappa_G$ ($\kappa_G \gtrsim 4$) materials the reversible magnetization curves can be approximated by straight lines stretching between $H = H_{c2}$ and $H = 0$ with $(\partial M/\partial H)_{Hc2}$ as given by Abrikosov.[51] That this must be the case can be seen from energy considerations, since for $\kappa \geq 4$, $2\kappa_2^2 - 1 \approx 2\kappa_2^2$ and the area $A$ under the magnetization curve must be $H_c^2/8\pi$, where $H_c$ is the thermodynamic critical field. According to Abrik-

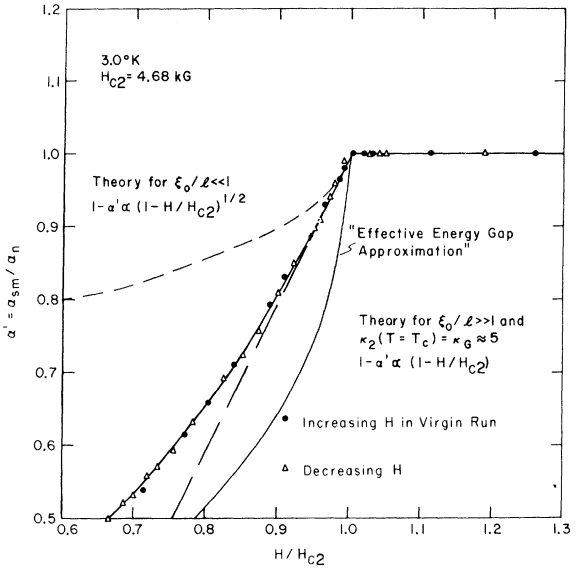


FIG. 9. Observed electronic attenuation $\alpha' = \alpha_{sm}/\alpha_n$ as a function of magnetic field near $H_{c2}$ at an intermediate temperature $T = 0.64T_c$ compared with theory for the clean $\xi_0/l \ll 1$ (upper dashed curve) and dirty $\xi_0/l \gg 1$ (lower dashed curve) limits and the predictions of the "effective energy-gap approximation."

osov,[51] $\partial M/\partial H = 1/4\pi(2\kappa_2^2 - 1)\beta$, $H_{c2} = \sqrt{2}\,\kappa_1 H_c$, and $\kappa_1 = \kappa_2$, $\beta \approx 1$, all independent of $T$. Thus, the straight-line approximation yields $A = \frac{1}{2}H_{c2}M(H=0) = \frac{1}{2}H_c^2\,\partial M/\partial H = H_c^2/8\pi$. Therefore, Eq. (3) is rewritten as

$$\alpha_{sm}/\alpha_n = 2/(1+e^x)\ , \tag{10}$$

$$x = \frac{\bar{\Delta}_0(H,T)}{k_BT} = \frac{\bar{\Delta}_0(H,T)}{\Delta_0(0,T)}\,\frac{\Delta_0(0,T)}{k_BT} = \left(\frac{M(H,T)}{M(0,T)}\right)^{1/2}\frac{\Delta_0(0,T)}{\Delta_{00}} \times 1.75\,\frac{T_c}{T}\ , \tag{11a}$$

$$\Delta_{00} \equiv \Delta_0(0,0)\ .$$

Since the Abrikosov-Maki parameter $\kappa_2$ is given by $M = (H - H_{c2})/4\pi(2\kappa_2^2 - 1)\beta$, substitution into Eq. (11) yields

$$x = \left(\frac{H_{c2}-H}{H_{c2}}\right)^{1/2}\frac{\Delta_0(0,T)}{\Delta_{00}} \times 1.75\,\frac{T_c}{T}\ . \tag{11b}$$

From the published[45] value of $\Delta_0(0,T)/\Delta_{00}$, the measured $\Delta_{00}/k_B$, the measured $T_c/T$, and Eq. (11), the attenuation ratio $\alpha_{sm}/\alpha_n$ was calculated and compared with the data. As is seen on Fig. 9, the calculated results plotted for an intermediate temperature are in poorer agreement with the data than the aforementioned dirty-limit theory.[7,21,22]

### 5. *Ultrasonic Attenuation for Weak Magnetic Fields $H_{fp} < H$*

For weak magnetic fields, such that $Be\lambda^2 \ll 1$, the longitudinal-wave electronic attenuation $\alpha(H,T)/\alpha_n$ as a function of the applied magnetic field $B$ is given[20] in the dirty limit $\xi_0/l \gg 1$ by

$$\left(\frac{\alpha(H,T)}{\alpha_n} - \frac{\alpha_s}{\alpha_n}\right)_{BCS} = k(T)\,\frac{B}{H_{c2}}\ , \tag{12}$$

$$k(t) = A\kappa_G^{2/3}\frac{\Delta_0}{2k_BT}\cosh^2\frac{\Delta_0}{2k_BT}\ ,$$

where $\lambda$ is the penetration depth and $A$ is an unspecified proportionality constant. Equation (12) predicts a linear dependence of the attenuation on $B$. This is in agreement with the data shown in Fig. 11, which plot semilogarithmically $[\alpha(H,T) - \alpha(H=0,T)]/H$ as a function of the reduced field. From Eq. (12), the ultrasonic data for $H_{c2}$, $\kappa_G$, and $T_c$, plus the tabulated values for the energy gap, it was possible to calculate $[\alpha(H,T) - \alpha_s]/\alpha_n H$ for several temperatures. These values fitted to the data at $t = 0.88$ ($A = 0.31$) appear as solid horizontal straight-line segments in Fig. 11. As shown in Fig. 11 and later in Fig. 13, these theoretical values are in reasonable agreement with those obtained from the ultrasonic data for high values of $t$ but deviate for low values of $t$.

Another theoretical treatment[1] of the ultrasonic attenuation in pure limit ($\xi_0/l \ll 1$) materials considers the states localized in the vortex core where the gap for the excitations is very small. Each vortex line is assumed to be nearly equivalent to a normal metal cylinder of diameter $\xi_G$, whose axis is parallel to the applied magnetic field. The predictions[1] made for the range of temperatures where $T \ll T_c$ are that despite the "near-normality" of the core, the attenuation arising from the vortex core is extremely small (the coherence factor is found to have a very low value). Invoking a similar model, which separates core and noncore regions, suggests focusing on the attenuation per vortex line. Since $\kappa_G \approx 5$ for this material, $4\pi M \ll H$ in the range $0.2 < H/H_{c2} \ll 1.0$ [e.g., at $H = 0.5H_{c2}$, $4\pi M = (H - H_{c2})/(2\kappa_2^2 - 1)\beta \approx 0.009H_{c2} \ll H$], so that $H \approx B = N_v\phi_0$, where $N_v$ is the vortex density. Thus, the parameter $[\alpha(H,T) - \alpha(H=0,T)/H$ in Fig. 11 is approximately equal to the total attenuation per vortex line. A marked feature of Fig. 11 is that, for low fields $h' \ll 1.0$, the attenuation per vortex is nearly independent of $h'$ at a given $t$, as one might expect for a low-density lattice of weakly interacting vortices. At fields near $h' = 1.0$, the lattice density has presumably increased to the point that the vortices must be viewed as a collective ensemble of strongly interacting elements. This latter regime has

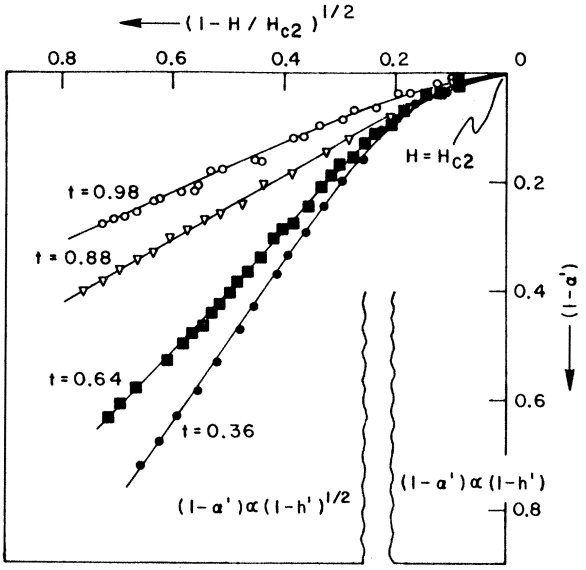


FIG. 10. Electronic attenuation $(1-\alpha')$ as a function of field $(1-H/H_{c2})^{1/2}$ where $\alpha'=\alpha_{sm}/\alpha_n$. Note that far away from $H_{c2}$ the data appear to agree well with pure limit $\xi_0/l \ll 1$ predictions that $(1-\alpha')\propto(1-h')^{1/2}$ where $h'=H/H_{c2}$.

been treated theoretically[7,21,22] and the predicted rise in attenuation and the slope at $h'=1.0$ as seen in Fig. 11 are then in good agreement with the data (see Sec. III C 3). The curves in Fig. 11 corresponding to low temperatures show shorter plateaus of constant $[\alpha(H,T)-\alpha(H=0)]/H$ than those at higher temperatures $T\approx T_c$. This is expected, because, at the lower temperatures, $H_{c2}$ and the magnetic field values $H$ over most of the curves are very high (see Fig. 2) giving rise to a correspondingly dense lattice of strongly interacting vortices. The interaction energy[52] between two vortex lines is predicted to be repulsive, decreases as $(1/\sqrt{S})\exp(-S/\lambda)$ at large distances $S$, and diverges as $\ln(\lambda/S)$ at short distances $S$ where $\lambda$ is the penetration depth. In Fig. 11 arrows indicate those points on the curves, where the attenuation per vortex line changes from being independent of $h'$ to increasing with $h'$. These points might be related to a critical spacing $S_c$ of the vortices, which in turn might be related to $\lambda$. If the vortex density is $N_v\approx H/\phi_0$, then $S\approx(H/\phi_0)^{-1/2}$. In the range of low temperatures (e.g., $t=0.36$, and $t=0.64$ in Fig. 11) the points marked by arrows occur at about the same $S$. An estimate for this spacing gives $S_c\approx 1.0\times10^{-5}$ cm. The penetration depth is given in the dirty limit $\xi_0/l\gg 1$ by[52-54]

$$\lambda(T)=0.61\lambda_L(0)\left(\frac{\xi_0}{l}\,\frac{T_c}{T_c-T}\right)^{1/2}, \qquad (13)$$

where the London penetration depth $\lambda_L(0)$ can be expressed as

$$\lambda_L(0)=1.33\times10^8\gamma^{1/2}[n^{2/3}S/S_f]^{-1}\ .$$

Evaluating as before (see Secs. III A and III B) gives $\lambda\approx 1.0\times10^{-5}$ cm in the same range of low temperatures, so that indeed $S_c\approx\lambda$ for $T\approx 0$. A more detailed comparison of the temperature dependences of $\lambda$ and $S_c$ is shown in Fig. 12.

It is interesting to note that above $H_{fp}$ the curve for $t=0.36$ in Fig. 11 can be approximated by two straight-line segments: One is the short plateau $(0.1\leq H/H_{c2}\leq 0.3)$ mentioned above; and the other $(0.3\leq H_{c2}\leq 1.0)$ suggests that near $T=0$ an analysis of $\alpha$ in terms of an exponential dependence on $H$ might be considered, similar to what has been proposed before.[19,27]

The slight initial decrease in the attenuation per vortex near $H=H_{fp}$, seen in Fig. 11 for the curves at $t=0.93$ and $t=0.88$, suggests a small contribution to the attenuation from scattering of quasiparticles from vortex lines, similar to what has been predicted and observed for clean type-II superconductors.[6,9,17,18]

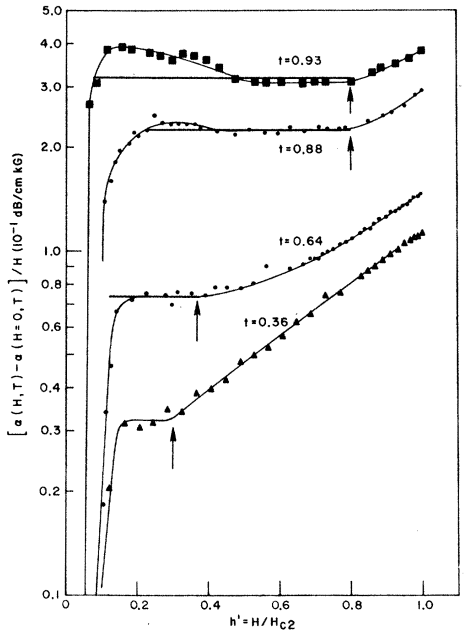


FIG. 11. Electronic attenuation per unit field $[\alpha(H,T)-\alpha(H=0,T)]/H$ as a function of field $H/H_{c2}$ for several temperatures on semilog plot. For fields $H_{fp}<H\leq H_{c2}$ the attenuation per unit field is approximately equal to the "electronic attenuation per vortex line." Note points indicated by arrows where attenuation changes from being linear in field to rising more rapidly than linear with field.

### 6. *Physical Interpretation of Regime of Weakly Interacting Vortex Lines*

In an effort to gain physical insight into the behavior of the attenuation in the regime of isolated weakly interacting vortex lines, a model was constructed in which vortices are replaced by cylinders for which the energy gap $\Delta_0(0, T)$ parameter is nearly zero. The matrix surrounding the cylinders acts with a BCS zero-field energy gap. If the normal core and matrix have nearly the same moduli, the total attenuation is given by

$$\alpha(H, T) = (\alpha_s + \alpha_B)[1 - V(H, T)] + (\alpha_n + \alpha_B) V(H, T) \quad (14)$$

where $V(T)$ is the total volume of normal material assumed to be made up of $N_v$ cores, each of diameter $D$ and unit length. Substituting Eq. (3) from Sec. III B, expressing $V$ in terms of $D$, and letting $N_v = B/\phi_0 \approx H/\phi_0$ gives

$$\alpha(H, T) \simeq (\alpha_s + \alpha_B) + \alpha_n \frac{\pi D^2}{4} \frac{H}{\phi_0} \tanh \frac{\Delta_0(0, T)}{2k_B T} \quad . \quad (15)$$

The slopes are given by

$$\frac{\alpha(H, T) - \alpha_s}{\alpha_n H} = \frac{\pi}{4} \frac{D^2}{\phi_0} \tanh \frac{\Delta_0}{2k_B T} \quad . \quad (16)$$

Recent theoretical calculations[55] of an effective core diameter, based on a vortex core model with a single vortex present, gave $D \approx \pi \xi_G$, where $\xi_G$ is the Ginzburg-Landau coherence distance which, for the dirty limit $\xi_0/l \gg 1$, is predicted[51,52] to be

$$\xi_G^2 \simeq 0.723\, \xi_0 l/(1 - T/T_c) \quad . \quad (17)$$

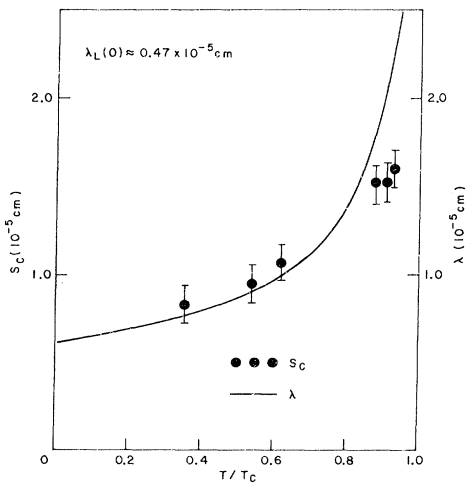


FIG. 12. Theoretical penetration depth $\lambda$ from Eq. (13) and critical vortex spacing $S_c$, corresponding to points indicated by arrows in Fig. 11, as a function of $T/T_c$.

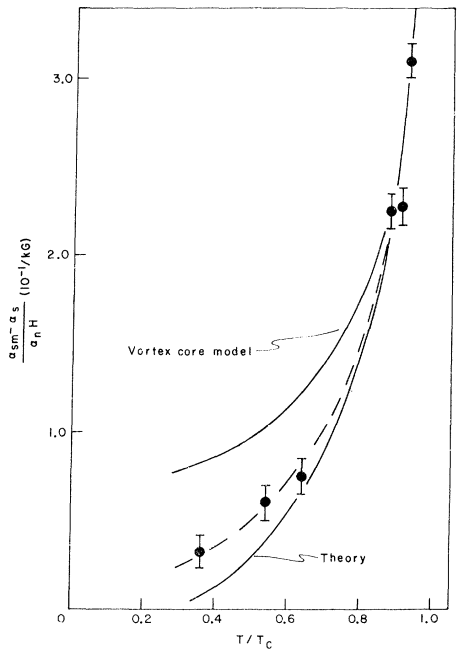


FIG. 13. Electronic attenuation per unit field $[\alpha(H, T) - \alpha(H = 0, T)]/H = (\alpha_{sm} - \alpha_s)/\alpha_n H$ as a function of temperature in the low magnetic field region $H_{fp} < H \ll H_{c2}$. The ultrasonic data are compared with theory (Ref. 20) and the results of a simple vortex core model.

The slope values from Eq. (16) could be fitted[56] to the corresponding experimental values over most of the temperature range for a choice of $D \approx 2\xi_G$, although the agreement near $T \gtrsim 0$ °K is poor. Thus, despite its simplicity, the model leads to the apparently correct linear magnetic field dependence, a qualitatively correct temperature dependence, and reasonable magnitudes for the attenuation. In the model, the linear field dependence is a consequence of a linear increase in vortex density with increasing field. The rapid increase in the slope values with temperature reflects the swelling of the vortex cores with temperature and consequently an increase in the volume of normal material at the expense of the volume of the superconducting matrix. A comparison between the data and the results of the simple vortex model is given in Fig. 13 which also shows the results of the theory.[20]

## IV. CONCLUSION

The behavior of the bulk specimen of $V$ – 5.6-at. % Ta in the superconducting state in zero applied field $H$ and in the normal state is in good agreement with the theory for an estimated $ql \approx 0.01$; the temperature dependence of the attenuation below $T_c$ is BCS-like with a zero-temperature ener-

gy gap $2\Delta(0,0) \approx 3.6 k_B T_c$. For magnetic field values close to the upper critical field $H_{c2}$, the field and temperature dependence of the attenuation agrees with the dirty-limit theory.

The only hysteresis observed in the ultrasonic measurements is near $H=0$ where some flux trapping can be expected. This high degree of magnetic reversibility makes it possible to interpret the data in the range $H \ll H_{c2}$. The field and temperature dependence of the attenuation appears to be in good agreement with the theory. Physical insight into the behavior in this regime could be obtained by a model which replaces vortices by cylinders in which the energy-gap parameter is nearly zero. The matrix surrounding the cylinders acts with a BCS zero-field energy gap.

The ultrasonic measurements furnished magnetically reversible values for the upper critical field $H_{c2}$ with a precision of better than 1%. The measured temperature dependence of the $H_{c2}$ values agrees well with the theory without $p$-wave scattering of electrons. The initial flux penetration is associated with a well-defined rise in attenuation. Some irreversibility and irregularity at this field value $H_{fp}$, however, suggest that $H_{fp}$ may be somewhat larger than the ideal lower critical field $H_{c1}$.

## ACKNOWLEDGMENTS

The author is indebted to R. R. Hake and J. A. Cape for their measurements of the resistivity and wishes to thank them, and G. Alers, H. E. Bömmel, H. Fink, D. Scalapino, L. Vredevoe, and S. Williamson for many helpful discussions. Special thanks go to H. Nadler for his crystal growth and sample preparation.

## APPENDIX

The following discussion describes the sample configuration, and modifications to the sample holder to achieve a small uniform demagnetization field.

As described in a previous paper,[31] the sample holder is a coaxial line, terminated at one end by the sample and collet. In the vicinity of this termination, the cylindrical center conductor of the coaxial line expands its diameter in a smooth transition, to end in a ball and socket configuration. The socket is formed by the electrode, which can swivel, so that its leveled and polished surface rests flatly on the quartz transducer bonded to the sample. The outer conductor of the coaxial line is also flared, so that a nearly constant proportion is maintained between $a$ and $b$, the diameters of the center and outer conductors. This arrangement is intended to assure a nearly constant characteristic impedance $Z_0$ ($\Omega$) which for a low-loss coaxial line is given by[57]

$$Z_0 = 60(\mu_1/\epsilon_1)^{1/2} \ln(b/a) \quad , \tag{A1}$$

where $\epsilon_1$ is the dielectric constant of the propagating medium and $\mu_1$ is the permeability of the medium separating the conductors. Figure 14 shows the sample holder in a cross-sectional diagram and the described features are apparent. Thus, from the point of view of maximum microwave power transmission, the design reduces the spatial distribution of electrical discontinuities, and allows a more effective matching of the single discontinuity at the transducer, which is accomplished with the coaxial double-stub tuners discussed previously.[31]

The geometry of the sample-electrode center-conductor configuration shown shaded in Fig. 14 is also ideally suited for magnetic measurements in the following way: The axis of symmetry of the cavity is aligned parallel to the applied magnetic field, given, for example, by a superconducting solonoid, such as shown in Fig. 14. The electrode

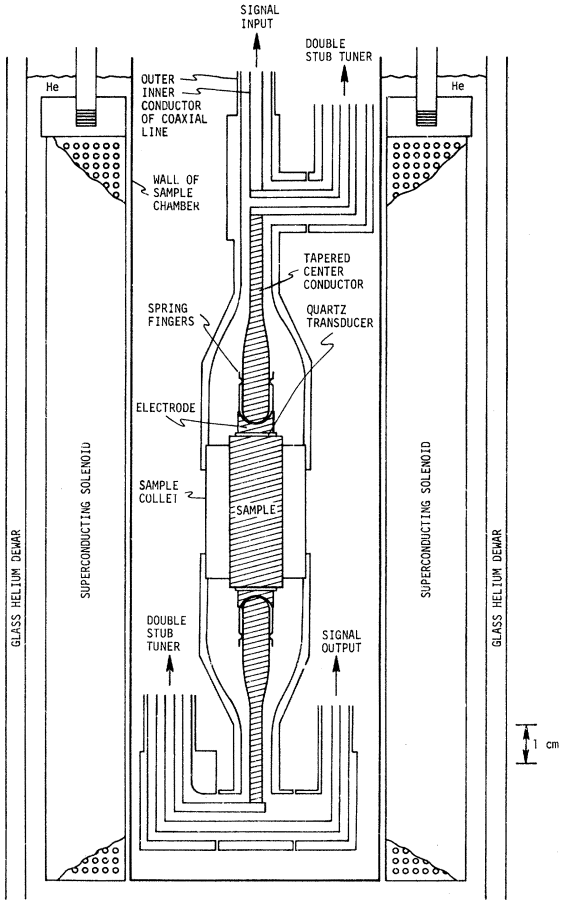


FIG. 14. Schematic drawing of tunable coaxial cavity useful from 0.4 to 4.0 GHz.

and center conductor combination is constructed to form, as nearly as possible, a solid, fashioned from sample material, in this case V-Ta alloy of nominally the same composition as the sample. All other parts of the cavity are fashioned from nonmagnetic metal, so that it may be assumed that the external applied field is uniform. Thus, the sample, electrode, and center conductors form, *in toto*, a prolate spheroid, i.e., an ellipsoid of revolution. As is well known, a uniformly magnetized ellipsoid produces a uniform demagnetization field, which is in turn consistent with a uniform induced magnetization. The situation in the mixed state of a superconductor is complicated by the fact that the magnetization is not uniform, but has a periodic vortex lattice structure. However, to the extent that the sample dimensions are large compared to the vortex spacing, it can be shown[33,58] that the demagnetization field for a spheroid in the mixed state, magnetized parallel to its symmetry axis, is given by

$$H_D = -4\pi n \langle m \rangle + (\text{correction terms}) \ , \qquad \text{(A2)}$$

where $n$ is the usual demagnetization factor corresponding to the symmetry direction and $\langle m \rangle$ is the volume average magnetization. The correction terms have been derived[58] for the most extreme case, an infinitely oblate spheroid, and shown to be negligible in general for all samples of bulk dimensions, i.e., large compared to the vortex lattice spacing. It may be concluded that in the mixed state, ellipsoids magnetize uniformly on a scale large compared to the vortex lattice spacing. An estimate of the demagnetization factor[34] for the combined configuration (maximum length $L = 15$ cm, maximum diameter $D = 1.3$ cm) gives $n_{\text{eff}} \approx 0.015$.


[1]C. Caroli and J. Matricon, Physik Kondensierten Materie 3, 380 (1965).

[2]L. N. Cooper, A. Houghton, and H. J. Lee, Phys. Rev. 148, 198 (1966); Phys. Rev. Letters 15, 584 (1965).

[3]K. Maki, Phys. Rev. 156, 437 (1967).

[4]F. B. McLean and A. Houghton, Phys. Letters 25A, 736 (1967).

[5]H. Kinder, Phys. Letters 26A, 319 (1968).

[6]R. M. Cleary, Phys. Rev. 175, 587 (1968).

[7]K. Maki, in *Superconductivity*, edited by R. D. Parks (Dekker, New York, 1969), Vol. II, p. 1035 [the factor $1/4\pi^2$ in Eq. 224 is in error and should read $1/8\pi^2$; this has been confirmed by K. Maki (private communication)].

[8]A. Ikushima, M. Fujii, and T. Suzuki, J. Phys. Chem. Solids 27, 327 (1965); A. I. Kishima, T. Suzuki, N. Tanaka, and S. Nakajima, J. Phys. Soc. Japan 19, 2235 (1964).

[9]E. M. Forgan and C. E. Gough, Phys. Letters 21, 133 (1966); 26A, 602 (1968).

[10]N. Tsuda, S. Koike, and T. Suzuki, Phys. Letters 22, 414 (1966).

[11]R. Kagiwada, M. Levy, and I. Rudnick, Phys. Letters 22, 29 (1966).

[12]R. Kagiwada, M. Levy, I. Rudnick, H. Kagiwada, and K. Maki, Phys. Rev. Letters 18, 74 (1967).

[13]M. Gottlieb, C. K. Jones, and M. Garbuny, Phys. Letters 25A, 107 (1967).

[14]A. Ikushima, K. Kajimura, and F. Akao, Phys. Letters 25A, 151 (1967).

[15]N. Tsuda and T. Suzuki, J. Phys. Chem. Solids 28, 2487 (1967).

[16]H. Kinder, Acustica 19, 160 (1967).

[17]A. C. E. Sinclair and J. R. Leibowitz, Phys. Rev. 175, 596 (1968).

[18]M. Gottlieb, M. Garbuny, and C. K. Jones, Phys. Letters 28A, 148 (1968).

[19]H. Ozaki, K. Kajimura, T. Ishiguro, N. Mikoshiba, Phys. Letters 28A, 300 (1968).

[20]V. P. Galaiko and I. I. Falko, Zh. Eksperim. i Teor. Fiz. 52, 976 (1967) [Soviet Phys. JETP 25, 646 (1967)].

[21]K. Maki and P. Fulde, Solid State Commun. 5, 21 (1967).

[22]F. B. McLean and A. Houghton, Phys. Rev. 157, 350 (1967).

[23]K. Maki, Phys. Rev. 148, 370 (1966).

[24]Y. Shapira and L. J. Neuringer, Phys. Rev. 154, 375 (1967); L. J. Neuringer and Y. Shapira, Phys. Rev. Letters 17, 81 (1966).

[25]R. R. Hake and W. G. Brammer, Phys. Rev. 133, A719 (1964).

[26]J. A. Cape, data for polycrystalline V – 5-at.% Ta (unpublished); L. J. Barnes and R. R. Hake (unpublished).

[27]B. R. Tittmann and H. E. Bömmel, Phys. Letters 28A, 396 (1968).

[28]E. Helfand and N. R. Werthamer, Phys. Rev. Letters 13, 686 (1968); Phys. Rev. 147, 288 (1966).

[29]N. R. Werthamer, E. Helfand, and P. C. Hohenberg, Phys. Rev. 147, 295 (1966).

[30]G. Eilenberger, Phys. Rev. 153, 584 (1967).

[31]B. R. Tittmann and H. E. Bömmel, Rev. Sci. Instr. 39, 614 (1968); 38, 1491 (1967).

[32]I. O. Kulik, Zh. Eksperim. i Teor. Fiz. Pis'ma v Redaktisyu 3, 395 (1966) [Soviet Phys. JETP Letters 3, 259 (1966)].

[33]J. A. Cape and J. M. Zimmerman, Phys. Rev. 153, 416 (1967).

[34]E. G. Stoner, Phil. Mag. 36, 803 (1945).

[35]C. Newton and D. L. Olson, Metallography 1, 249 (1968).

[36]See, e.g., R. W. Morse, in *Progress in Cryogenics I*, edited by K. R. Mendelsohn (Heywood, London, 1959).

[37]A. B. Pippard, *Reports on Progress in Physics* (The Institute of Physics and the Physical Society, London, 1960), Vol. XXIII, p. 176.

[38]R. R. Hake, Phys. Rev. 158, 356 (1967).

[39]T. G. Berlincourt and R. R. Hake, Phys. Rev. 131, 140 (1963).

[40]B. B. Goodman, Phys. Rev. Letters 6, 597 (1961).

[41]A. B. Pippard, Phys. Rev. 46, 1104 (1955).
[42]E. I. Blount, Phys. Rev. 114, 418 (1959).
[43]J. Bardeen, L. N. Copper, and J. R. Schrieffer, Phys. Rev. 108, 1175 (1957); J. Bardeen and J. R. Schrieffer, in *Progress in Low Temperature Physics III*, edited by C. J. Gorter (North-Holland, Amsterdam, 1967).
[44]T. Tsuneto, Phys. Rev. 121, 402 (1961).
[45]B. Mühlschlegel, Z. Physik 155, 313 (1959).
[46]W. A. Fate, R. W. Shaw, and G. L. Salinger, Phys. Rev. 172, 413 (1968).
[47]The $\gamma$ value is obtained from the calorimetric $\gamma = 1.10 \times 10^4$ ergs cm$^{-3}$°K$^{-2}$ by making an approximate correction for the $T_c$ difference of the calorimetric ($T_c = 4.3$ °K) and the ultrasonic specimens ($T_c = 4.7$ °K). We assume from BCS (Ref. 43) $d\gamma/\gamma = [\ln(0.85\Theta_D/T_c)]^{-1}\, dT_c/T_c = 0.24\, T_c$; this yields a $\gamma = 1.12 \times 10^4$ erg cm$^{-3}$ °K$^{-2}$.
[48]G. Lasher, Phys. Rev. 140, A523 (1965).
[49]K. Maki (private communication).
[50]L. Dubeck, P. Lindenfeld, E. A. Lynton, and H. Rohrer, Phys. Rev. Letters 10, 98 (1963).
[51]A. A. Abrikosov, Zh. Eksperim. i Teor. Fiz. 32, 1442 (1957) [Soviet Phys. JETP 5, 1174 (1957)].
[52]See, e.g., P. G. de Gennes, *Superconductivity of Metals and Alloys*, translated by P. A. Pincus (Benjamin, New York, 1966).
[53]C. Caroli, P. G. de Gennes, and J. Matricon, Physik Kondensierten Materie 1, 176 (1963).
[54]H. J. Fink and A. G. Presson (unpublished) point out an apparent error in the numerical constant on the right-hand side of Eq. (12), i.e., the constant should read 0.61 instead of 0.64.
[55]A. G. Van Vijfeijken, Philips Res. Rept. Suppl. 8 (1968).
[56]Note, by combing Eqs. (1) and (4) (Secs. III A and III B1), the expression for $\xi_0 l$ simplifies to $\xi_0 l = 1.0 \times 10^{-12}/\rho_n \gamma T_c$ [see Ref. 38, Eq. (A8)].
[57]See, for example, T. Moreno, *Microwave Transmission Design Data* (Dover, New York, 1958).
[58]J. A. Cape, Phys. Rev. 179, 485 (1969).

PHYSICAL REVIEW B VOLUME 2, NUMBER 3 1 AUGUST 1970

# Enhancement of the Anomalous-Skin-Effect Fields beneath a Rough Surface and Its Effect on the Correlation-Produced Magnetoplasma Peak

G. A. Baraff
*Bell Telephone Laboratories, Murray Hill, New Jersey* 07974
(Received 9 January 1970)

The surface-roughness model, which describes the surface impedance of potassium as a function of the strength of the magnetic field normal to the surface, is used here to calculate the deep-field enhancement factor – i.e., the amount by which the field deep in the bulk of a rough-surfaced sample exceeds that in the bulk of a diffuse-surfaced sample. Having obtained this factor, we recalculate the change in surface impedance caused by Fermi-liquid effects, using the enhanced field in the calculation rather than the original diffuse field. This procedure should yield the change in surface impedance caused by correlations among the conduction electrons in a sample having a rough surface. We find that the peak in surface resistance calculated in this way is fully comparable in size with what has been observed, and that its location is very close to $\omega_c/\omega = (1 + A_2)^{-1}$, where $A_2$ is the second Landau-theory Fermi-liquid parameter. The value of $A_2$ deduced in this way is $-0.03$, in agreement with the value deduced by Platzman, Walsh, and Fòo from their theory and observation of the high-frequency waves.

## I. INTRODUCTION

Recent measurements of the surface resistance of potassium in the anomalous-skin-effect regime[1,2] exhibit a dependence on the strength of the magnetic field which can only be understood on the assumption that the mean free path for electrons close to the surface is much shorter than the mean free path for electrons deeper in the bulk of the sample.[3] They also exhibit a resonancelike anomaly which has been ascribed[1,4] to excitation of the correlation-produced magnetoplasma mode.[5] Attempts to calculate the existence, size, and magnetic field dependence of this anomaly have met with only partial success: If one assumes specular scattering for electrons at the surface, the calculated size of the anomaly is about $10^{-4}$ of what is observed.[1] If one assumes diffuse scattering, the calculated size rises to about $10^{-2}$ of what is observed, but the anomaly seems to have the wrong phase.[4] In this paper, we shall show that the same surface-roughness model,[3] and approximately the same parameters which are needed to explain the magnetic field dependence of the surface resis-